PHYSICAL REVIEW D **93,** 092008 (2016)

Measurement of the $B_s^0 \to D_s^{(*)+} D_s^{(*)-}$ branching fractions

R. Aaij *et al.*[*]
(LHCb Collaboration)

(Received 25 February 2016; published 20 May 2016)

The branching fraction of the decay $B_s^0 \to D_s^{(*)+} D_s^{(*)-}$ is measured using pp collision data corresponding to an integrated luminosity of 1.0 fb^{-1}, collected using the LHCb detector at a center-of-mass energy of 7 TeV. It is found to be $\mathcal{B}(B_s^0 \to D_s^{(*)+} D_s^{(*)-}) = (3.05 \pm 0.10 \pm 0.20 \pm 0.34)\%$, where the uncertainties are statistical, systematic, and due to the normalization channel, respectively. The branching fractions of the individual decays corresponding to the presence of one or two $D_s^{*\pm}$ are also measured. The individual branching fractions are found to be $\mathcal{B}(B_s^0 \to D_s^{*\pm} D_s^{\mp}) = (1.35 \pm 0.06 \pm 0.09 \pm 0.15)\%$, $\mathcal{B}(B_s^0 \to D_s^{*+} D_s^{*-}) = (1.27 \pm 0.08 \pm 0.10 \pm 0.14)\%$. All three results are the most precise determinations to date.

DOI: 10.1103/PhysRevD.93.092008

I. INTRODUCTION

Because of $B_s^0 - \bar{B}_s^0$ oscillations, the mass and flavor eigenstates of the B_s^0 system do not coincide. The B_s^0 meson mass eigenstates have a relative decay width difference $\Delta\Gamma_s/\Gamma_s$, where $\Delta\Gamma_s$ (Γ_s) is the difference (average) of the decay widths between the heavy and light states. The relative decay width difference is one of the key parameters of the B_s^0 system, and its precise determination allows stringent tests of the flavor sector of the standard model.

Under certain theoretical assumptions, $B_s^0 \to D_s^{(*)+} D_s^{(*)-}$ decays were thought to saturate the CP-even contribution to $\Delta\Gamma_s$, and therefore the branching fraction of $B_s^0 \to D_s^{(*)+} D_s^{(*)-}$ was used as a means of approximating $\Delta\Gamma_s/\Gamma_s$ [1]. This approximation is now considered to be a poor one [2], as the decay modes containing at least one $D_s^{*\pm}$ have a non-negligible CP-odd component, and other three-body B_s^0 decays can contribute to the value of $\Delta\Gamma_s$ at a similar level as $B_s^0 \to D_s^{(*)+} D_s^{(*)-}$ decays. A detailed discussion of theoretical predictions of the $B_s^0 \to D_s^{(*)+} D_s^{(*)-}$ branching fractions, and the predicted contribution of other modes to the value of $\Delta\Gamma_s/\Gamma_s$, is given in Ref. [3].

In a more general context, since the branching fraction of $B_s^0 \to D_s^{(*)+} D_s^{(*)-}$ decays is one of the dominant contributions to the total inclusive $b \to c\bar{c}s$ branching fraction, its precise measurement is an important ingredient in model-independent searches for physics beyond the standard model in B meson decays [4]. The most recent measurements are provided by the Belle [5], CDF [6], and D0 [7] collaborations who obtain, respectively,

$$\mathcal{B}(B_s^0 \to D_s^{(*)+} D_s^{(*)-}) = (4.32^{+0.42+1.04}_{-0.39-1.03})\%,$$
$$\mathcal{B}(B_s^0 \to D_s^{(*)+} D_s^{(*)-}) = (3.38 \pm 0.25 \pm 0.30 \pm 0.56)\%,$$
$$\mathcal{B}(B_s^0 \to D_s^{(*)+} D_s^{(*)-}) = (3.5 \pm 1.0 \pm 1.1)\%.$$

The data used in the analysis presented in this paper correspond to an integrated luminosity of 1.0 fb^{-1}, collected by the LHCb experiment during the 2011 run period. The branching fraction of the full $B_s^0 \to D_s^{(*)+} D_s^{(*)-}$ decay is determined relative to the $B^0 \to D_s^+ D^-$ decay, which has a similar final state and a precisely measured branching fraction. The charm daughters are reconstructed using the $D_s^+ \to K^+K^-\pi^+$ and $D^- \to K^+\pi^-\pi^-$ final states. Throughout the paper, unless stated otherwise, charge-conjugate modes are implied and summed over. The branching fraction ratio is determined as

$$\frac{\mathcal{B}(B_s^0 \to D_s^{(*)+} D_s^{(*)-})}{\mathcal{B}(B^0 \to D_s^+ D^-)} = \frac{f_d}{f_s} \cdot \frac{\epsilon^{B^0}}{\epsilon^{B_s^0}} \cdot \frac{\mathcal{B}(D^- \to K^+\pi^-\pi^-)}{\mathcal{B}(D_s^+ \to K^-K^+\pi^+)} \cdot \frac{N_{B_s^0}}{N_{B^0}}, \quad (1)$$

where f_d (f_s) is the fraction of $\bar{B}^0$ ($\bar{B}_s^0$) mesons produced in the fragmentation of a b quark, $\epsilon^{B^0}/\epsilon^{B_s^0}$ is the relative efficiency of the B^0 to the B_s^0 selections, $\mathcal{B}(D^- \to K^+\pi^-\pi^-)$ and $\mathcal{B}(D_s^+ \to K^-K^+\pi^+)$ are the branching fractions of the charm daughter decays, and $N_{B_s^0}/N_{B^0}$ is the relative yield of B_s^0 and B^0 candidates.

The branching fraction of the exclusive $B_s^0 \to D_s^{*+} D_s^{*-}$ decay is determined in the same way, along with the branching fraction of $B_s^0 \to D_s^{*\pm} D_s^{\mp}$. The branching fraction of the $B_s^0 \to D_s^+ D_s^-$ decay has been previously measured by LHCb using the same data as this analysis [8], and

[*]Full author list given at the end of the article.

is therefore not determined in this study. However, the selection efficiency and yield in the $B_s^0 \to D_s^+ D_s^-$ channel are determined in this analysis, as both are needed for the calculation of the total $B_s^0 \to D_s^{(*)+} D_s^{(*)-}$ selection efficiency.

II. DETECTOR AND SIMULATION

The LHCb detector [9,10] is a single-arm forward spectrometer covering the pseudorapidity range $2 < \eta < 5$, designed for the study of particles containing b or c quarks. The detector includes a high-precision tracking system consisting of a silicon-strip vertex detector surrounding the pp interaction region, a large-area silicon-strip detector located upstream of a dipole magnet with a bending power of about 4 Tm, and three stations of silicon-strip detectors and straw drift tubes placed downstream of the magnet. The tracking system provides a measurement of momentum, p, of charged particles with a relative uncertainty that varies from 0.5% at low momentum to 1.0% at 200 GeV/c. The minimum distance of a track to a primary vertex, the impact parameter, is measured with a resolution of $(15 + 29/p_{\mathrm{T}})$ μm, where p_{T} is the component of the momentum transverse to the beam, in GeV/c. Different types of charged hadrons are distinguished using information from two ring-imaging Cherenkov detectors. Photons, electrons and hadrons are identified by a calorimeter system consisting of scintillating-pad and preshower detectors, an electromagnetic calorimeter and a hadronic calorimeter. Muons are identified by a system composed of alternating layers of iron and multiwire proportional chambers. The event selection is performed in two stages, with an initial online selection followed by a tighter offline selection. The online event selection is performed by a trigger [11], which consists of a hardware stage, based on information from the calorimeter and muon systems, followed by a software stage, which performs a full event reconstruction.

In the simulation, pp collisions are generated using Pythia 6 [12] with a specific LHCb configuration [13]. Decays of hadronic particles are described by EvtGen [14], in which final-state radiation is generated using Photos [15]. The interaction of the generated particles with the detector, and its response, are implemented using the Geant4 toolkit [16] as described in Ref. [17].

III. SIGNAL SELECTION

The D_s^{*+} meson decays to a D_s^+ meson and either a photon or a neutral pion $(93.5 \pm 0.7)\%$ and $(5.8 \pm 0.7)\%$ of the time, respectively, nearly saturating the total branching fraction. The remainder of the decays are ignored in this analysis. Neither of the neutral particles is reconstructed in the decay chain, and the individual $B_s^0 \to D_s^{*\pm} D_s^{\mp}$ and $B_s^0 \to D_s^{*+} D_s^{*-}$ decays are identified through the reconstructed invariant mass of the $D_s^+ D_s^-$ system. The individual peaks from $B_s^0 \to D_s^{*\pm}(\to D_s^{\pm}\gamma) D_s^{\mp}$ and $B_s^0 \to D_s^{*\pm}(\to D_s^{\pm}\pi^0) D_s^{\mp}$ are not resolved. Therefore the reconstructed $D_s^+ D_s^-$ mass distribution has three separate peaks, corresponding to decays containing zero, one, or two $D_s^{*\pm}$ particles.

At the hardware trigger stage, events are required to have a muon with high p_{T} or a hadron, photon or electron with high transverse energy in the calorimeters. For hadrons, the transverse energy threshold is 3.5 GeV. Candidate B_s^0 and B^0 mesons are used in the analysis if at least one of the associated tracks is selected by the hardware trigger, or if the event is triggered independently of the particles in the signal decay. The software trigger considers all charged particles with $p_{\mathrm{T}} > 500$ MeV/c and constructs two-, three-, or four-track secondary vertices which require a significant displacement from the primary pp interaction vertices. At least one charged particle must have a transverse momentum $p_{\mathrm{T}} > 1.7$ GeV/c and be inconsistent with originating from a primary vertex. A multivariate algorithm [18] is used for the identification of secondary vertices consistent with the decay of a b hadron. The selection to this point is hereafter referred to as the initial selection.

Signal B_s^0 and normalization $B^0 \to D_s^+ D^-$ candidates are required to satisfy a number of additional conditions in order to be included in the final samples. Kaons and pions are required to be identified by the particle identification (PID) system. All D_s^+ and D^- candidates must have an invariant mass within ± 30 MeV/c^2 of their known values [19]. Signal B_s^0 candidates are required to have a reconstructed mass in the range 4750–5800 MeV/c^2, whereas B^0 candidates must have a mass in the range 5050–5500 MeV/c^2. After these requirements are applied there are still contributions from other b -hadron decays into final states with two charm particles. The decays $\Lambda_b^0 \to \Lambda_c^+(\to pK^-\pi^+) D_s^-$, where the p is misidentified as a K^+, and $B^0 \to D_s^+ D^-(\to K^+\pi^-\pi^-)$, where a π^- is misidentified as a K^-, result in background contamination in the signal channel, while the decay $B_s^0 \to D_s^+ D_s^-$ contributes to the background in the normalization channel if the K^+ in $D_s^+ \to K^+K^-\pi^+$ is misidentified as a π^+. As these backgrounds accumulate in reconstructed mass close to the signal peaks, candidates consistent with any one of these background decay hypotheses are rejected in the selection by applying a veto based on the invariant mass of the candidate under the alternative particle type hypotheses. Candidate D_s^+ mesons are vetoed if they have a reconstructed mass in the range 2271–2301 MeV/c^2 when the K^+ candidate is assumed to be a proton, or a mass in the range 1835–1905 MeV/c^2 when the K^+ candidate is assigned the π^+ mass. Candidate D^- mesons are vetoed if they have a reconstructed mass in the range 1950–1990 MeV/c^2 when a π^- candidate is assigned the kaon mass. In a simulated sample of $B^0 \to D_s^+ D^-$ decays, 17.7% of the events meet all of the $B_s^0 \to D_s^{(*)+} D_s^{(*)-}$

TABLE I. Efficiencies of the various selection criteria for the three individual channels of $B_s^0 \to D_s^{(*)+} D_s^{(*)-}$, and for $B^0 \to D_s^+ D^-$. Each efficiency is presented relative to the previous cut and measured using simulated events, except for the PID efficiency which is obtained from data. The D_s^+ veto was only applied to the normalization mode, $B^0 \to D_s^+ D^-$.

	Selection efficiency (%)			
Selection	$B_s^0 \to D_s^+ D_s^-$	$B_s^0 \to D_s^{*\pm} D_s^{\mp}$	$B_s^0 \to D_s^{*+} D_s^{*-}$	$B^0 \to D_s^+ D^-$
Reconstruction	0.1184 ± 0.0003	0.1127 ± 0.0005	0.1061 ± 0.0005	0.1071 ± 0.0002
Initial selection	1.362 ± 0.008	1.250 ± 0.010	1.100 ± 0.010	1.416 ± 0.009
Mass requirements	89.4 ± 0.6	87.8 ± 1.0	88.3 ± 1.0	88.5 ± 0.6
BDT	97.9 ± 0.7	96.6 ± 1.1	96.7 ± 1.1	97.6 ± 0.7
D^+ veto	48.7 ± 0.5	50.3 ± 0.8	48.9 ± 0.8	68.7 ± 0.6
D_s^+ veto	—	—	—	64.8 ± 0.7
Λ_c^+ veto	96.3 ± 1.0	96.3 ± 1.6	95.9 ± 1.6	98.2 ± 0.8
Trig. requirement	96.6 ± 0.7	96.7 ± 1.1	96.6 ± 1.1	96.8 ± 0.7
PID requirements	82.4 ± 0.2	82.4 ± 0.2	82.4 ± 0.2	84.2 ± 0.1
Total	0.0527 ± 0.0067	0.0460 ± 0.0095	0.0372 ± 0.0081	0.0467 ± 0.0060

selection criteria before the $D^{\pm}$ veto is applied. After the veto, only 0.05% of the simulated $B^0 \to D_s^+ D^-$ sample still pass the full $B_s^0 \to D_s^{(*)+} D_s^{(*)-}$ selection. The decay $B^0 \to D_s^+ D_s^-$ and three-body $B^{\pm} \to D_{(s)}^+ D_{(s)}^- h^{\pm}$ decays, where h is either a kaon or pion, are examined as other potential background sources, but are all disregarded because of either a small selection efficiency or small branching fraction relative to the signal channels.

In order to further improve the purity of the signal and normalization samples, a boosted decision tree (BDT) classifier is used to distinguish real $B_{(s)}^0$ decays from combinatorial background [20]. The BDT is trained using the AdaBoost algorithm [21] to distinguish simulated B_s^0 signal decays from background candidates obtained from mass sidebands in the data. Background candidates must contain a B_s^0 candidate with a mass greater than 5600 MeV/c^2 and two $D_s^{\pm}$ candidates with masses less than 1930 MeV/c^2 or greater than 2010 MeV/c^2. The set of 14 variables used as input to the BDT exploits the topology of the B_s^0 decay chain and includes the transverse momentum of the B_s^0 candidate and of the two $D_s^{\pm}$ daughters, as well as the product of the absolute transverse momenta of the pions and kaons produced in the decay of each $D_s^{\pm}$. The decay times of the two $D_s^{\pm}$ candidates with respect to the primary vertex and variables related to the consistency of the B_s^0 and of the two $D_s^{\pm}$ to come from the primary vertex are also used. The optimal BDT requirement is chosen to maximize the value of $N_s/\sqrt{N_s + N_b}$, where N_s is the total number of signal candidates matching any of the three exclusive decays in $B_s^0 \to D_s^{(*)+} D_s^{(*)-}$ and N_b is the total number of combinatorial background events as taken from the fit. The same BDT classifier and selection criteria are also applied to the normalization sample.

TABLE II. Efficiency of the normalization channel $B^0 \to D_s^+ D^-$ relative to the signal decays.

Channel	$\epsilon^{B^0}/\epsilon^{B_s^0}$
$B_s^0 \to D_s^+ D_s^-$	0.89 ± 0.02
$B_s^0 \to D_s^{*\pm} D_s^{\mp}$	1.02 ± 0.03
$B_s^0 \to D_s^{*+} D_s^{*-}$	1.26 ± 0.03
$B_s^0 \to D_s^{(*)+} D_s^{(*)-}$	1.06 ± 0.02

The efficiencies of the selection criteria in both the signal and normalization channels are listed in Table I. The efficiencies of the background vetoes, trigger, reconstruction, and BDT selection are determined using simulated signal samples. The efficiencies of identifying K^+ and π^+ mesons are determined using a calibration data sample of $D^{*+} \to D^0(\to K^-\pi^+)\pi^+$ decays, with kinematic quantities reweighted to match those of the signal candidates. The efficiency of the PID selection is found to be $(82.4 \pm 0.2)\%$ for signal B_s^0 decays and $(84.2 \pm 0.1)\%$ for B^0 decays. The efficiency of the full $B_s^0 \to D_s^{(*)+} D_s^{(*)-}$ decay is determined by calculating a weighted average of the individual signal channels, with weights given by the relative yields in data. The relative efficiencies of the B^0 decay to the three individual channels and the full decay are given in Table II.

IV. SIGNAL AND BACKGROUND SHAPES

The B_s^0 and B^0 yields in the signal channels and the normalization mode are extracted by performing a three-dimensional extended unbinned maximum likelihood fit to the mass distributions of the $B_{(s)}^0$ meson and the two charm daughters.

In order to determine the yields for the individual signal peaks, the B_s^0 candidate mass distribution in each channel is modeled using simulated signal events. The $B_s^0 \to D_s^+ D_s^-$ peak is parametrized as the sum of a Crystal Ball function [22] and a Gaussian function. The tail parameters of the Crystal Ball function, the ratio of the width of its Gaussian core to the width of the Gaussian function, and the relative weight of each function in the full distribution, are taken

from simulation. The mean and width of the Gaussian core are allowed to float. The two $D_s^{\pm}$ distributions are also parametrized using this model, with all shape parameters fixed to the values found in simulation.

Because of the kinematic differences between the $D_s^{*+} \to D_s^+\gamma$ and $D_s^{*+} \to D_s^+\pi^0$ decays, the peak of the $B_s^0 \to D_s^{*\pm}D_s^{\mp}$ mass distribution is parametrized by a superposition of two Gaussian functions. The individual mean values, the ratio of the widths, and the fraction of each Gaussian function in the full distribution are fixed to values taken from simulation. The peak corresponding to $B_s^0 \to D_s^{*+}D_s^{*-}$ decays is modeled using a single Gaussian function, with the mean fixed to the value found from simulated events.

There is also a component in the fit to describe the presence of background decays of the form $B_s^0 \to D_{sJ}^+D_s^-$, where the D_{sJ}^+ can be either a $D_{s1}(2460)^+$ or a $D_{s0}(2317)^+$ meson that decays to a D_s^+ along with some combination of photons and neutral or charged pions. As some decay products are missed, this background is present only at the low mass region of the signal distribution. The shape of the distribution is determined by fitting to $B_s^0 \to D_{s1}(2460)^+D_s^-$ simulated events, as the contribution from $D_{s1}(2460)^+$ is currently the best understood among the D_{sJ}^+ decays. It is found to be well modeled by an Argus function [23], all shape parameters for which are fixed to the values found in simulation.

The combinatorial background shape in the B_s^0 candidate mass distribution is parametrized by a second-order polynomial, and the model is validated with candidates passing a wrong-sign version of the selection. The wrong-sign selection is identical to the signal selection but instead looks for events containing two D_s^+ mesons. The parameters of the combinatorial background distribution are allowed to float in the full fit to data, and are found to be compatible with the values obtained from the fit to the wrong-sign sample. The combinatorial background shape in the $D_s^{\pm}$ distribution is determined using events taken from the high-mass sideband region of the B_s^0 distribution, and is found to be consistent with a first-order polynomial. The impact of adding a small Gaussian contribution to account for the presence of real $D_s^{\pm}$ mesons in the combinatorial background was found to be minimal, with the observed deviations from the nominal signal yields being smaller than the statistical uncertainty in each case.

The B^0 distribution is modeled using the same parametrization as for the full B_s^0 distribution, with one exception. The peak where either the D_s^+ or D^- comes from the decay of an excited state is modeled by a superposition of three Gaussian functions, rather than the two-Gaussian model used in the B_s^0 case, to account for the difference in distributions from D_s^{*+} and D^{*-} decays, as the D^{*-} decay contains a π^0 in the final state more frequently than D_s^{*+} decays. There is also a small contribution from the decay $B_s^0 \to D_s^-D^+$, which is modeled with the same distribution as for the signal B_s^0 candidates.

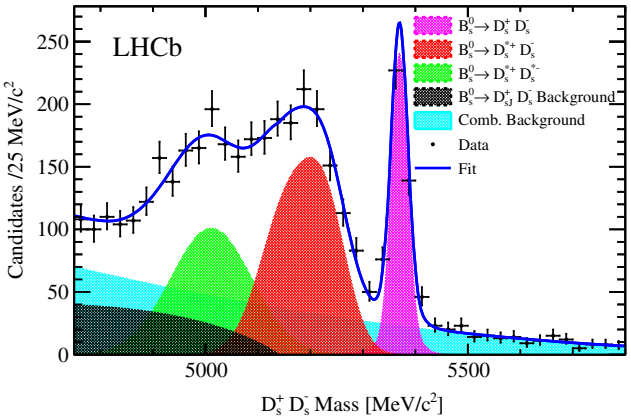

FIG. 1. Invariant mass distribution of the $B_s^0 \to D_s^{(*)+}D_s^{(*)-}$ candidates. Also shown is the fit function and the individual components of the fit model.

V. FIT RESULTS

The fit to the signal data samples is shown in Fig. 1, where the triple peaked structure of the full decay is clearly visible. The yields for the individual signal channels and the two backgrounds are given in Table III. The total $B_s^0 \to D_s^{(*)+}D_s^{(*)-}$ yield is the sum of the individual signal channel yields, with the uncertainty calculated using the correlation coefficients between the individual yields, and is found to be 2230 ± 63. The full fit to the data sample for the normalization mode is shown in Fig. 2, and the yields are given in Table IV. Almost all $B^0 \to D_s^{*\pm}D^{*\mp}$ decays are reconstructed with a mass lower than the 5050 MeV/c^2 mass cut imposed on the B^0 candidates. There is thus a relatively small yield from this channel. Only the main $B^0 \to D_s^+D^-$ peak is used for normalization purposes.

VI. SYSTEMATIC UNCERTAINTIES

A number of systematic uncertainties affect the measurements of the ratios of branching fractions; the sources and magnitudes of these uncertainties are summarized in Table V. The dominant source of uncertainty for two of the three branching fractions comes from the b fragmentation fraction ratio, $f_s/f_d = 0.259 \pm 0.015$ [24]. Part of the uncertainty on this ratio is due to the ratio of the charm branching fractions $B(D_s^+ \to K^+K^-\pi^+)/B(D^- \to K^+\pi^-\pi^-) = 0.594 \pm 0.020$

TABLE III. The yields extracted from the fit to the $B_s^0 \to D_s^{(*)+}D_s^{(*)-}$ candidate sample.

Decay Mode	Yield
$B_s^0 \to D_s^+D_s^-$	412 ± 23
$B_s^0 \to D_s^{*\pm}D_s^{\mp}$	1032 ± 39
$B_s^0 \to D_s^{*\pm}D_s^{*\mp}$	786 ± 48
Combinatorial background	1342 ± 47
$B_s^0 \to D_s(2460)^{\pm}D_s^{\mp}$	432 ± 42

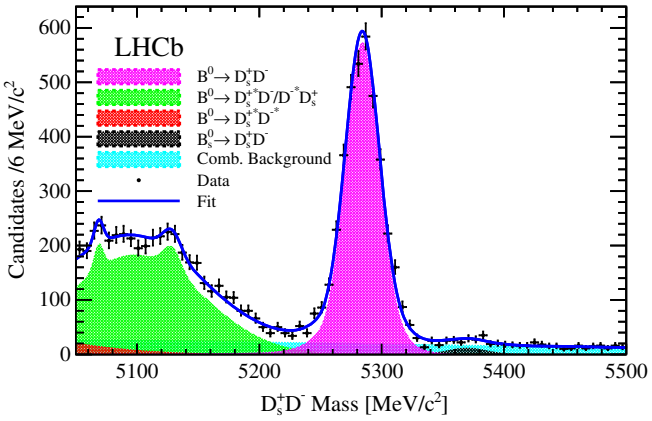

FIG. 2. Invariant mass distribution of the $B^0 \to D_s^{(*)\pm} D^{(*)\mp}$ candidates. Also shown is the fit function and the individual components of the fit model.

[24], the inverse of which is used in the measurements presented in this paper, as shown in Eq. (1). With the two values from Ref. [24], the part of the uncertainty on f_s/f_d due to the charm branching fractions cancels, leading to a total uncertainty for the product $f_d/f_s \times B(D^- \to K^+\pi^-\pi^-)/B(D_s^+ \to K^+K^-\pi^+)$ of 4.7%.

The fit model used for the yield extraction is validated using pseudoexperiments and is found to be unbiased. The uncertainty due to the imperfect knowledge of the shape of the full mass distribution is investigated by measuring the yields using alternative models for each of the peaks. The $D_s^+ D_s^-$ peak is modeled with an Apollonios function [25] or a Cruijff function [26], the $D_s^{*\pm} D_s^{\mp}$ peak is modeled using a single Gaussian function, and the $D_s^{*+} D_s^{*-}$ peak is modeled using a combination of two Gaussian functions. The $B^0 \to D_s^{(*)\pm} D^{(*)\mp}$ fit model uncertainty is assessed by modeling the $B^0 \to D_s^- D^+$ peak with both an Apollonios function and a Cruijff function. In all cases, the systematic uncertainty is taken to be the RMS deviation of the sets of yields with respect to the nominal yields found using the standard fits. The $B^0 \to D_s^- D^+$ uncertainty is added in quadrature to the signal channel uncertainties, leading to a systematic uncertainty of 3.4% for the $D_s^{*\pm} D_s^{\mp}$ branching fraction ratio, 2.2% for the $D_s^{*+} D_s^{*-}$ branching fraction ratio, and 2.2% for the total $B_s^0 \to D_s^{(*)+} D_s^{(*)-}$ branching fraction ratio.

The uncertainty on the combinatorial background yield is determined by considering the differences when instead fitting this background with an exponential function, and is of the order of 1.5% for all of the branching fraction ratios.

The dominant uncertainty for the $B_s^0 \to D_s^{*+} D_s^{*-}$ decay channel results from the lack of knowledge of the $B_s^0 \to D_{sJ}^+ D_s^-$ background decays. The shape of this background overlaps mostly with the $B_s^0 \to D_s^{*+} D_s^{*-}$ signal decays, and therefore the systematic uncertainty due to this background shape is much larger for this channel (5.0%) than for the other two exclusive branching fractions (0.2%–0.4%). The uncertainty is measured by repeating the fit with the cutoff point of the Argus function varied from 5050 MeV/c^2 to 5200 MeV/c^2, where the upper limit is chosen in order to account for the presence of decays containing $D_{s0}(2317)^+$ mesons. The changes to the yields from the values found in the nominal fit are calculated in each case. The systematic uncertainty in each channel is then assigned as the RMS of the full set of deviations. The uncertainty on the overall branching fraction ratio is also determined in this way, and is found to be 1.9%.

The uncertainties on the overall efficiencies due to the limited size of the simulated samples are calculated individually for each channel. For the total measurement, $\mathcal{B}(B_s^0 \to D_s^{(*)+} D_s^{(*)-})$, a weighted average of the individual uncertainties is used, with weights proportional to the final

TABLE IV. The yields extracted from the fit to the $B^0 \to D_s^{(*)\pm} D^{(*)\mp}$ candidate sample.

Decay Mode	Yield
$B^0 \to D_s^+ D^-$	3636 ± 64
$B^0 \to D_s^{*+} D^-/D^{*-} D_s^+$	3579 ± 110
$B^0 \to D_s^{*+} D^{*-}$	166 ± 86
$B_s^0 \to D_s^{\pm} D^{\mp}$	85 ± 13
Combinatorial background	1542 ± 56

TABLE V. Systematic uncertainties, in % of the relevant branching fraction ratio, for the $B_s^0 \to D_s^{(*)+} D_s^{(*)-}$ branching fraction ratios.

Source	$B_s^0 \to D_s^{*\pm} D_s^{\mp}$	$B_s^0 \to D_s^{*+} D_s^{*-}$	$B_s^0 \to D_s^{(*)+} D_s^{(*)-}$
$f_d/f_s \times \frac{B(D^- \to K^+\pi^-\pi^-)}{B(D_s^+ \to K^+K^-\pi^+)}$	4.7	4.7	4.7
Fit model	3.4	2.2	2.2
Comb. background	1.2	1.9	1.5
D_{sJ}^+ background	0.4	5.0	1.9
Simulation statistics	1.9	2.1	1.9
PID efficiency	1.4	1.8	1.5
Trigger efficiency	1.5	1.5	1.5
Total	6.6	8.1	6.4

yield values obtained from data. These uncertainties on the efficiencies are then propagated to the branching fraction ratios.

There is a systematic uncertainty arising from the calculation of the efficiencies of the PID cuts. The calibration of the data samples is performed in bins of momentum and pseudorapidity, which results in an uncertainty on the calculated efficiencies owing to the finite size of the $D^{*+} \to D^0\pi^+$ calibration samples and the binning scheme used. The uncertainty resulting from the calibration sample size and binning scheme is determined by redoing the calibration using different binning schemes. Another systematic uncertainty is due to the presence of a small combinatorial background component in the samples that are used to determine the PID efficiencies. The systematic uncertainty due to this contamination is estimated by comparing the efficiencies found in data to those found when calibrating simulated signal events. The total uncertainties due to the PID efficiency calculation for the three branching fraction ratios presented in this paper are shown in Table V. The value for $B_s^0 \to D_s^{(*)+}D_s^{(*)-}$ is again the weighted average of the contributing channels, with the uncertainty for the $D_s^+D_s^-$ contribution being 1.1%.

The uncertainty of 1.5% from the trigger response is assessed by considering variations in the response between data and simulation. The individual uncertainties are combined in quadrature to give the total relative systematic uncertainties for each measurement given in Table V.

VII. SUMMARY AND DISCUSSION

Inserting the measured yields and relative efficiencies into Eq. (1), along with the f_s/f_d and $B(D^- \to K^+\pi^-\pi^-)/B(D_s^+ \to K^+K^-\pi^+)$ values taken from [24], gives

$$\frac{\mathcal{B}(B_s^0 \to D_s^{(*)+}D_s^{(*)-})}{\mathcal{B}(B^0 \to D_s^+D^-)} = 4.24 \pm 0.14(\text{stat}) \pm 0.27(\text{syst}),$$
$$\frac{\mathcal{B}(B_s^0 \to D_s^{*\pm}D_s^{\mp})}{\mathcal{B}(B^0 \to D_s^+D^-)} = 1.88 \pm 0.08(\text{stat}) \pm 0.12(\text{syst}),$$
$$\frac{\mathcal{B}(B_s^0 \to D_s^{*+}D_s^{*-})}{\mathcal{B}(B^0 \to D_s^+D^-)} = 1.76 \pm 0.11(\text{stat}) \pm 0.14(\text{syst}).$$

Using the current world average measurement of the $B^0 \to D_s^+D^-$ branching fraction of $(7.2 \pm 0.8) \times 10^{-3}$ [19], gives

$$\mathcal{B}(B_s^0 \to D_s^{(*)+}D_s^{(*)-}) = (3.05 \pm 0.10 \pm 0.20 \pm 0.34)\%,$$
$$\mathcal{B}(B_s^0 \to D_s^{*\pm}D_s^{\mp}) = (1.35 \pm 0.06 \pm 0.09 \pm 0.15)\%,$$
$$\mathcal{B}(B_s^0 \to D_s^{*+}D_s^{*-}) = (1.27 \pm 0.08 \pm 0.10 \pm 0.14)\%,$$

where the uncertainties are statistical, systematic, and due to the branching fraction of the normalization channel, respectively.

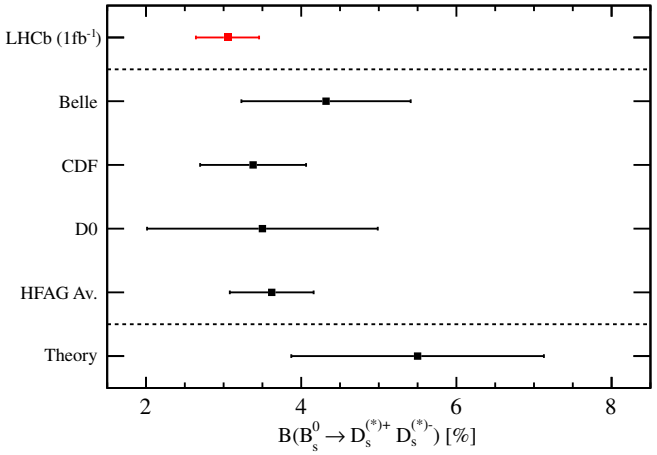

FIG. 3. The $B_s^0 \to D_s^{(*)+}D_s^{(*)-}$ branching fraction measurements by Belle, CDF, and D0, the current world average, the theoretical prediction from Ref. [3], and the new LHCb result.

Figure 3 shows the LHCb measurement of the total $B_s^0 \to D_s^{(*)+}D_s^{(*)-}$ branching fraction, along with the previous measurements by Belle [5], CDF [6], and D0 [7], the average of these previous measurements as calculated by HFAG [27], and the theoretical value from Ref. [3]. The theoretical prediction is for a decay time $t = 0$, while the measurements integrate over the B_s^0 meson lifetime; the correction factor for mixing is known [28], but has not been applied. The LHCb result is consistent with all previous measurements and calculations, and is the most precise determination to date. In addition, the LHCb measurements of the individual $B_s^0 \to D_s^{*\pm}D_s^{\mp}$ and $B_s^0 \to D_s^{*+}D_s^{*-}$ branching fractions are consistent with, and more precise than, all previous measurements.

Using this measurement of the branching fraction of $B_s^0 \to D_s^{(*)+}D_s^{(*)-}$ decays to calculate $\Delta\Gamma_s/\Gamma_s$ as detailed in Ref. [1] gives a value approximately half as large as the most recent HFAG determination [27], suggesting that indeed $B_s^0 \to D_s^{(*)+}D_s^{(*)-}$ decays do not saturate the CP-even modes [2]. The measurements presented in this analysis will be useful in improving the understanding of hadronization effects in B_s^0 decays via the $b \to c\bar{c}s$ quark transition, and in determining a precise value of the inclusive branching fraction of these $b \to c\bar{c}s$ decays.

ACKNOWLEDGMENTS

We express our gratitude to our colleagues in the CERN accelerator departments for the excellent performance of the LHC. We thank the technical and administrative staff at the LHCb institutes. We acknowledge support from CERN and from the national agencies: CAPES, CNPq, FAPERJ and FINEP (Brazil); NSFC (China); CNRS/IN2P3 (France); BMBF, DFG and MPG (Germany); INFN (Italy); FOM and NWO (The Netherlands); MNiSW and NCN

(Poland); MEN/IFA (Romania); MinES and FANO (Russia); MinECo (Spain); SNSF and SER (Switzerland); NASU (Ukraine); STFC (United Kingdom); NSF (USA). We acknowledge the computing resources that are provided by CERN, IN2P3 (France), KIT and DESY (Germany), INFN (Italy), SURF (The Netherlands), PIC (Spain), GridPP (United Kingdom), RRCKI and Yandex LLC (Russia), CSCS (Switzerland), IFIN-HH (Romania), CBPF (Brazil), PL-GRID (Poland) and OSC (USA). We are indebted to the communities behind the multiple open source software packages on which we depend. Individual groups or members have received support from AvH Foundation (Germany), EPLANET, Marie Skłodowska-Curie Actions and ERC (European Union), Conseil Général de Haute-Savoie, Labex ENIGMASS and OCEVU, Région Auvergne (France), RFBR and Yandex LLC (Russia), GVA, XuntaGal and GENCAT (Spain), The Royal Society, Royal Commission for the Exhibition of 1851 and the Leverhulme Trust (United Kingdom).

[1] R. Aleksan, A. Le Yaouanc, L. Oliver, O. Pène, and J.-C. Raynal, Estimation of $\Delta\Gamma_s$ for the $B_s^0 - \bar{B}_s^0$ system. Exclusive decays and the parton model, Phys. Lett. B **316**, 567 (1993).

[2] A. Lenz, Theoretical update of B-Mixing and Lifetimes, arXiv:1205.1444.

[3] C.-K. Chua, W.-S. Hou, and C.-H. Shen, Long-distance contribution to $\Delta\Gamma_s/\Gamma_s$ of the B_s^0-$\bar{B}_s^0$ system, Phys. Rev. D **84**, 074037 (2011).

[4] F. Krinner, A. Lenz, and T. Rauh, The inclusive decay $b \to c\bar{c}s$ revisited, Nucl. Phys. **B876**, 31 (2013).

[5] S. Esen *et al.* (Belle Collaboration), Precise measurement of the branching fractions for $B_s \to D_s^{(*)+} D_s^{(*)-}$ and first measurement of the $D_s^{*+} D_s^{*-}$ polarization using e^+e^- collisions, Phys. Rev. D **87**, 031101 (2013).

[6] T. Aaltonen *et al.* (CDF Collaboration), Measurement of $B_s^0 \to D_s^{(*)+} D_s^{(*)-}$ Branching Ratios, Phys. Rev. Lett. **108**, 201801 (2012).

[7] V. M. Abazov *et al.* (D0 Collaboration), Evidence for Decay $B_s^0 \to D_s^{(*)} D_s^{(*)}$ and a Measurement of $\Delta\Gamma_s^{CP}/\Gamma_s$, Phys. Rev. Lett. **102**, 091801 (2009).

[8] R. Aaij *et al.* (LHCb Collaboration), First observations of $\bar{B}_s^0 \to D^+D^-$, $D_s^+D^-$ and $D^0\bar{D}^0$ decays, Phys. Rev. D **87**, 092007 (2013).

[9] A. A. Alves Jr. *et al.* (LHCb Collaboration), The LHCb detector at the LHC, J. Instrum. **3**, S08005 (2008).

[10] R. Aaij *et al.* (LHCb Collaboration), LHCb detector performance, Int. J. Mod. Phys. A **30**, 1530022 (2015).

[11] R. Aaij *et al.*, The LHCb trigger and its performance in 2011, J. Instrum. **8**, P04022 (2013).

[12] T. Sjöstrand, S. Mrenna, and P. Skands, PYTHIA 6.4 physics and manual, J. High Energy Phys. 05 (2006) 026.

[13] I. Belyaev *et al.*, Handling of the generation of primary events in Gauss, the LHCb simulation framework, J. Phys. Conf. Ser. **331**, 032047 (2011).

[14] D. J. Lange, The EvtGen particle decay simulation package, Nucl. Instrum. Methods Phys. Res., Sect. A **462**, 152 (2001).

[15] P. Golonka and Z. Was, PHOTOS Monte Carlo: A precision tool for QED corrections in Z and W decays, Eur. Phys. J. C **45**, 97 (2006).

[16] J. Allison *et al.* (Geant4 Collaboration), Geant4 developments and applications, IEEE Trans. Nucl. Sci. **53**, 270 (2006); S. Agostinelli *et al.* (Geant4 Collaboration), Geant4: A simulation toolkit, Nucl. Instrum. Methods Phys. Res., Sect. A **506**, 250 (2003).

[17] M. Clemencic, G. Corti, S Easo, C. R Jones, S. Miglioranzi, M. Pappagallo, and P. Robbe, The LHCb simulation application, Gauss: Design, evolution and experience, J. Phys. Conf. Ser. **331**, 032023 (2011).

[18] V. V. Gligorov and M. Williams, Efficient, reliable and fast high-level triggering using a bonsai boosted decision tree, J. Instrum. **8**, P02013 (2013).

[19] K. A. Olive *et al.* (Particle Data Group Collaboration), Review of particle physics, Chin. Phys. C **38**, 090001 (2014), and 2015 update.

[20] L. Breiman, J. H. Friedman, R. A. Olshen, and C. J. Stone, *Classification and Regression Trees* (Wadsworth International Group, Belmont, California, USA, 1984).

[21] R. E. Schapire and Y. Freund, A decision-theoretic generalization of on-line learning and an application to boosting, J. Comput. Syst. Sci. **55**, 119 (1997).

[22] T. Skwarnicki, Ph.D. thesis, Institute of Nuclear Physics, Krakow, 1986; Report No. DESY-F31-86-02.

[23] H. Albrecht *et al.* (ARGUS Collaboration), Search for hadronic $b \to u$ decays, Phys. Lett. B **241**, 278 (1990).

[24] LHCb Collaboration, Report No. LHCb-CONF-2013-011.

[25] D. M. Santos and F. Dupertuis, Mass distributions marginalized over per-event errors, Nucl. Instrum. Methods Phys. Res., Sect. A **764**, 150 (2014).

[26] P. del Amo Sanchez *et al.* (*BABAR* Collaboration), Study of $B \to X\gamma$ decays and determination of $|V_{td}/V_{ts}|$, Phys. Rev. D **82**, 051101 (2010).

[27] Y. Amhis *et al.* (Heavy Flavor Averaging Group Collaboration), Averages of b-hadron, c-hadron, and τ-lepton properties as of summer 2014, arXiv:1412.7515, updated results and plots available at http://www.slac.stanford.edu/xorg/hfag/.

[28] K. De Bruyn, R. Fleischer, R. Knegjens, P. Koppenburg, M. Merk, and N. Tuning, Branching ratio measurements of B_s decays, Phys. Rev. D **86**, 014027 (2012).

R. Aaij,[39] C. Abellán Beteta,[41] B. Adeva,[38] M. Adinolfi,[47] A. Affolder,[53] Z. Ajaltouni,[5] S. Akar,[6] J. Albrecht,[10] F. Alessio,[39] M. Alexander,[52] S. Ali,[42] G. Alkhazov,[31] P. Alvarez Cartelle,[54] A. A. Alves Jr,[58] S. Amato,[2] S. Amerio,[23] Y. Amhis,[7] L. An,[3,40] L. Anderlini,[18] G. Andreassi,[40] M. Andreotti,[17,a] J. E. Andrews,[59] R. B. Appleby,[55] O. Aquines Gutierrez,[11] F. Archilli,[39] P. d'Argent,[12] A. Artamonov,[36] M. Artuso,[60] E. Aslanides,[6] G. Auriemma,[26,b] M. Baalouch,[5] S. Bachmann,[12] J. J. Back,[49] A. Badalov,[37] C. Baesso,[61] W. Baldini,[17,39] R. J. Barlow,[55] C. Barschel,[39] S. Barsuk,[7] W. Barter,[39] V. Batozskaya,[29] V. Battista,[40] A. Bay,[40] L. Beaucourt,[4] J. Beddow,[52] F. Bedeschi,[24] I. Bediaga,[1] L. J. Bel,[42] V. Bellee,[40] N. Belloli,[21,c] I. Belyaev,[32] E. Ben-Haim,[8] G. Bencivenni,[19] S. Benson,[39] J. Benton,[47] A. Berezhnoy,[33] R. Bernet,[41] A. Bertolin,[23] M.-O. Bettler,[39] M. van Beuzekom,[42] S. Bifani,[46] P. Billoir,[8] T. Bird,[55] A. Birnkraut,[10] A. Bizzeti,[18,d] T. Blake,[49] F. Blanc,[40] J. Blouw,[11] S. Blusk,[60] V. Bocci,[26] A. Bondar,[35] N. Bondar,[31,39] W. Bonivento,[16] S. Borghi,[55] M. Borisyak,[66] M. Borsato,[38] T. J. V. Bowcock,[53] E. Bowen,[41] C. Bozzi,[17,39] S. Braun,[12] M. Britsch,[12] T. Britton,[60] J. Brodzicka,[55] N. H. Brook,[47] E. Buchanan,[47] C. Burr,[55] A. Bursche,[41] J. Buytaert,[39] S. Cadeddu,[16] R. Calabrese,[17,a] M. Calvi,[21,c] M. Calvo Gomez,[37,e] P. Campana,[19] D. Campora Perez,[39] L. Capriotti,[55] A. Carbone,[15,f] G. Carboni,[25,g] R. Cardinale,[20,h] A. Cardini,[16] P. Carniti,[21,c] L. Carson,[51] K. Carvalho Akiba,[2] G. Casse,[53] L. Cassina,[21,c] L. Castillo Garcia,[40] M. Cattaneo,[39] Ch. Cauet,[10] G. Cavallero,[20] R. Cenci,[24,i] M. Charles,[8] Ph. Charpentier,[39] M. Chefdeville,[4] S. Chen,[55] S.-F. Cheung,[56] N. Chiapolini,[41] M. Chrzaszcz,[41,27] X. Cid Vidal,[39] G. Ciezarek,[42] P. E. L. Clarke,[51] M. Clemencic,[39] H. V. Cliff,[48] J. Closier,[39] V. Coco,[39] J. Cogan,[6] E. Cogneras,[5] V. Cogoni,[16,j] L. Cojocariu,[30] G. Collazuol,[23,k] P. Collins,[39] A. Comerma-Montells,[12] A. Contu,[39] A. Cook,[47] M. Coombes,[47] S. Coquereau,[8] G. Corti,[39] M. Corvo,[17,a] B. Couturier,[39] G. A. Cowan,[51] D. C. Craik,[51] A. Crocombe,[49] M. Cruz Torres,[61] S. Cunliffe,[54] R. Currie,[54] C. D'Ambrosio,[39] E. Dall'Occo,[42] J. Dalseno,[47] P. N. Y. David,[42] A. Davis,[58] O. De Aguiar Francisco,[2] K. De Bruyn,[6] S. De Capua,[55] M. De Cian,[12] J. M. De Miranda,[1] L. De Paula,[2] P. De Simone,[19] C.-T. Dean,[52] D. Decamp,[4] M. Deckenhoff,[10] L. Del Buono,[8] N. Déléage,[4] M. Demmer,[10] D. Derkach,[66] O. Deschamps,[5] F. Dettori,[39] B. Dey,[22] A. Di Canto,[39] F. Di Ruscio,[25] H. Dijkstra,[39] S. Donleavy,[53] F. Dordei,[39] M. Dorigo,[40] A. Dosil Suárez,[38] A. Dovbnya,[44] K. Dreimanis,[53] L. Dufour,[42] G. Dujany,[55] K. Dungs,[39] P. Durante,[39] R. Dzhelyadin,[36] A. Dziurda,[27] A. Dzyuba,[31] S. Easo,[50,39] U. Egede,[54] V. Egorychev,[32] S. Eidelman,[35] S. Eisenhardt,[51] U. Eitschberger,[10] R. Ekelhof,[10] L. Eklund,[52] I. El Rifai,[5] Ch. Elsasser,[41] S. Ely,[60] S. Esen,[12] H. M. Evans,[48] T. Evans,[56] A. Falabella,[15] C. Färber,[39] N. Farley,[46] S. Farry,[53] R. Fay,[53] D. Ferguson,[51] V. Fernandez Albor,[38] F. Ferrari,[15] F. Ferreira Rodrigues,[1] M. Ferro-Luzzi,[39] S. Filippov,[34] M. Fiore,[17,39,a] M. Fiorini,[17,a] M. Firlej,[28] C. Fitzpatrick,[40] T. Fiutowski,[28] F. Fleuret,[7,l] K. Fohl,[39] P. Fol,[54] M. Fontana,[16] F. Fontanelli,[20,h] D. C. Forshaw,[60] R. Forty,[39] M. Frank,[39] C. Frei,[39] M. Frosini,[18] J. Fu,[22] E. Furfaro,[25,g] A. Gallas Torreira,[38] D. Galli,[15,f] S. Gallorini,[23] S. Gambetta,[51] M. Gandelman,[2] P. Gandini,[56] Y. Gao,[3] J. García Pardiñas,[38] J. Garra Tico,[48] L. Garrido,[37] D. Gascon,[37] C. Gaspar,[39] R. Gauld,[56] L. Gavardi,[10] G. Gazzoni,[5] D. Gerick,[12] E. Gersabeck,[12] M. Gersabeck,[55] T. Gershon,[49] Ph. Ghez,[4] S. Gianì,[40] V. Gibson,[48] O. G. Girard,[40] L. Giubega,[30] V. V. Gligorov,[39] C. Göbel,[61] D. Golubkov,[32] A. Golutvin,[54,39] A. Gomes,[1,m] C. Gotti,[21,c] M. Grabalosa Gándara,[5] R. Graciani Diaz,[37] L. A. Granado Cardoso,[39] E. Graugés,[37] E. Graverini,[41] G. Graziani,[18] A. Grecu,[30] E. Greening,[56] P. Griffith,[46] L. Grillo,[12] O. Grünberg,[64] B. Gui,[60] E. Gushchin,[34] Yu. Guz,[36,39] T. Gys,[39] T. Hadavizadeh,[56] C. Hadjivasiliou,[60] G. Haefeli,[40] C. Haen,[39] S. C. Haines,[48] S. Hall,[54] B. Hamilton,[59] X. Han,[12] S. Hansmann-Menzemer,[12] N. Harnew,[56] S. T. Harnew,[47] J. Harrison,[55] J. He,[39] T. Head,[40] V. Heijne,[42] A. Heister,[9] K. Hennessy,[53] P. Henrard,[5] L. Henry,[8] J. A. Hernando Morata,[38] E. van Herwijnen,[39] M. Heß,[64] A. Hicheur,[2] D. Hill,[56] M. Hoballah,[5] C. Hombach,[55] W. Hulsbergen,[42] T. Humair,[54] M. Hushchyn,[66] N. Hussain,[56] D. Hutchcroft,[53] D. Hynds,[52] M. Idzik,[28] P. Ilten,[57] R. Jacobsson,[39] A. Jaeger,[12] J. Jalocha,[56] E. Jans,[42] A. Jawahery,[59] M. John,[56] D. Johnson,[39] C. R. Jones,[48] C. Joram,[39] B. Jost,[39] N. Jurik,[60] S. Kandybei,[44] W. Kanso,[6] M. Karacson,[39] T. M. Karbach,[39,†] S. Karodia,[52] M. Kecke,[12] M. Kelsey,[60] I. R. Kenyon,[46] M. Kenzie,[39] T. Ketel,[43] E. Khairullin,[66] B. Khanji,[21,39,c] C. Khurewathanakul,[40] T. Kirn,[9] S. Klaver,[55] K. Klimaszewski,[29] O. Kochebina,[7] M. Kolpin,[12] I. Komarov,[40] R. F. Koopman,[43] P. Koppenburg,[42,39] M. Kozeiha,[5] L. Kravchuk,[34] K. Kreplin,[12] M. Kreps,[49] P. Krokovny,[35] F. Kruse,[10] W. Krzemien,[29] W. Kucewicz,[27,n] M. Kucharczyk,[27] V. Kudryavtsev,[35] A. K. Kuonen,[40] K. Kurek,[29] T. Kvaratskheliya,[32] D. Lacarrere,[39] G. Lafferty,[55,39] A. Lai,[16] D. Lambert,[51] G. Lanfranchi,[19] C. Langenbruch,[49] B. Langhans,[39] T. Latham,[49] C. Lazzeroni,[46] R. Le Gac,[6] J. van Leerdam,[42] J.-P. Lees,[4] R. Lefèvre,[5] A. Leflat,[33,39] J. Lefrançois,[7] E. Lemos Cid,[38] O. Leroy,[6] T. Lesiak,[27] B. Leverington,[12] Y. Li,[7] T. Likhomanenko,[66,65] M. Liles,[53] R. Lindner,[39] C. Linn,[39] F. Lionetto,[41] B. Liu,[16] X. Liu,[3] D. Loh,[49] I. Longstaff,[52] J. H. Lopes,[2] D. Lucchesi,[23,k] M. Lucio Martinez,[38] H. Luo,[51] A. Lupato,[23] E. Luppi,[17,a] O. Lupton,[56] N. Lusardi,[22] A. Lusiani,[24] F. Machefert,[7] F. Maciuc,[30] O. Maev,[31] K. Maguire,[55] S. Malde,[56] A. Malinin,[65]

G. Manca,[7] G. Mancinelli,[6] P. Manning,[60] A. Mapelli,[39] J. Maratas,[5] J. F. Marchand,[4] U. Marconi,[15] C. Marin Benito,[37] P. Marino,[24,39,i] J. Marks,[12] G. Martellotti,[26] M. Martin,[6] M. Martinelli,[40] D. Martinez Santos,[38] F. Martinez Vidal,[67] D. Martins Tostes,[2] L. M. Massacrier,[7] A. Massafferri,[1] R. Matev,[39] A. Mathad,[49] Z. Mathe,[39] C. Matteuzzi,[21] A. Mauri,[41] B. Maurin,[40] A. Mazurov,[46] M. McCann,[54] J. McCarthy,[46] A. McNab,[55] R. McNulty,[13] B. Meadows,[58] F. Meier,[10] M. Meissner,[12] D. Melnychuk,[29] M. Merk,[42] E Michielin,[23] D. A. Milanes,[63] M.-N. Minard,[4] D. S. Mitzel,[12] J. Molina Rodriguez,[61] I. A. Monroy,[63] S. Monteil,[5] M. Morandin,[23] P. Morawski,[28] A. Mordà,[6] M. J. Morello,[24,i] J. Moron,[28] A. B. Morris,[51] R. Mountain,[60] F. Muheim,[51] D. Müller,[55] J. Müller,[10] K. Müller,[41] V. Müller,[10] M. Mussini,[15] B. Muster,[40] P. Naik,[47] T. Nakada,[40] R. Nandakumar,[50] A. Nandi,[56] I. Nasteva,[2] M. Needham,[51] N. Neri,[22] S. Neubert,[12] N. Neufeld,[39] M. Neuner,[12] A. D. Nguyen,[40] T. D. Nguyen,[40] C. Nguyen-Mau,[40,o] V. Niess,[5] R. Niet,[10] N. Nikitin,[33] T. Nikodem,[12] A. Novoselov,[36] D. P. O'Hanlon,[49] A. Oblakowska-Mucha,[28] V. Obraztsov,[36] S. Ogilvy,[52] O. Okhrimenko,[45] R. Oldeman,[16,48,j] C. J. G. Onderwater,[68] B. Osorio Rodrigues,[1] J. M. Otalora Goicochea,[2] A. Otto,[39] P. Owen,[54] A. Oyanguren,[67] A. Palano,[14,p] F. Palombo,[22,q] M. Palutan,[19] J. Panman,[39] A. Papanestis,[50] M. Pappagallo,[52] L. L. Pappalardo,[17,a] C. Pappenheimer,[58] W. Parker,[59] C. Parkes,[55] G. Passaleva,[18] G. D. Patel,[53] M. Patel,[54] C. Patrignani,[20,h] A. Pearce,[55,50] A. Pellegrino,[42] G. Penso,[26,r] M. Pepe Altarelli,[39] S. Perazzini,[15,f] P. Perret,[5] L. Pescatore,[46] K. Petridis,[47] A. Petrolini,[20,h] M. Petruzzo,[22] E. Picatoste Olloqui,[37] B. Pietrzyk,[4] M. Pikies,[27] D. Pinci,[26] A. Pistone,[20] A. Piucci,[12] S. Playfer,[51] M. Plo Casasus,[38] T. Poikela,[39] F. Polci,[8] A. Poluektov,[49,35] I. Polyakov,[32] E. Polycarpo,[2] A. Popov,[36] D. Popov,[11,39] B. Popovici,[30] C. Potterat,[2] E. Price,[47] J. D. Price,[53] J. Prisciandaro,[38] A. Pritchard,[53] C. Prouve,[47] V. Pugatch,[45] A. Puig Navarro,[40] G. Punzi,[24,s] W. Qian,[4] R. Quagliani,[7,47] B. Rachwal,[27] J. H. Rademacker,[47] M. Rama,[24] M. Ramos Pernas,[38] M. S. Rangel,[2] I. Raniuk,[44] N. Rauschmayr,[39] G. Raven,[43] F. Redi,[54] S. Reichert,[55] A. C. dos Reis,[1] V. Renaudin,[7] S. Ricciardi,[50] S. Richards,[47] M. Rihl,[39] K. Rinnert,[53,39] V. Rives Molina,[37] P. Robbe,[7,39] A. B. Rodrigues,[1] E. Rodrigues,[55] J. A. Rodriguez Lopez,[63] P. Rodriguez Perez,[55] S. Roiser,[39] V. Romanovsky,[36] A. Romero Vidal,[38] J. W. Ronayne,[13] M. Rotondo,[23] T. Ruf,[39] P. Ruiz Valls,[67] J. J. Saborido Silva,[38] N. Sagidova,[31] B. Saitta,[16,j] V. Salustino Guimaraes,[2] C. Sanchez Mayordomo,[67] B. Sanmartin Sedes,[38] R. Santacesaria,[26] C. Santamarina Rios,[38] M. Santimaria,[19] E. Santovetti,[25,g] A. Sarti,[19,r] C. Satriano,[26,b] A. Satta,[25] D. M. Saunders,[47] D. Savrina,[32,33] S. Schael,[9] M. Schiller,[39] H. Schindler,[39] M. Schlupp,[10] M. Schmelling,[11] T. Schmelzer,[10] B. Schmidt,[39] O. Schneider,[40] A. Schopper,[39] M. Schubiger,[40] M.-H. Schune,[7] R. Schwemmer,[39] B. Sciascia,[19] A. Sciubba,[26,r] A. Semennikov,[32] A. Sergi,[46] N. Serra,[41] J. Serrano,[6] L. Sestini,[23] P. Seyfert,[21] M. Shapkin,[36] I. Shapoval,[17,44,a] Y. Shcheglov,[31] T. Shears,[53] L. Shekhtman,[35] V. Shevchenko,[65] A. Shires,[10] B. G. Siddi,[17] R. Silva Coutinho,[41] L. Silva de Oliveira,[2] G. Simi,[23,s] M. Sirendi,[48] N. Skidmore,[47] T. Skwarnicki,[60] E. Smith,[56,50] E. Smith,[54] I. T. Smith,[51] J. Smith,[48] M. Smith,[55] H. Snoek,[42] M. D. Sokoloff,[58,39] F. J. P. Soler,[52] F. Soomro,[40] D. Souza,[47] B. Souza De Paula,[2] B. Spaan,[10] P. Spradlin,[52] S. Sridharan,[39] F. Stagni,[39] M. Stahl,[12] S. Stahl,[39] S. Stefkova,[54] O. Steinkamp,[41] O. Stenyakin,[36] S. Stevenson,[56] S. Stoica,[30] S. Stone,[60] B. Storaci,[41] S. Stracka,[24,i] M. Straticiuc,[30] U. Straumann,[41] L. Sun,[58] W. Sutcliffe,[54] K. Swientek,[28] S. Swientek,[10] V. Syropoulos,[43] M. Szczekowski,[29] T. Szumlak,[28] S. T'Jampens,[4] A. Tayduganov,[6] T. Tekampe,[10] G. Tellarini,[17,a] F. Teubert,[39] C. Thomas,[56] E. Thomas,[39] J. van Tilburg,[42] V. Tisserand,[4] M. Tobin,[40] J. Todd,[58] S. Tolk,[43] L. Tomassetti,[17,a] D. Tonelli,[39] S. Topp-Joergensen,[56] N. Torr,[56] E. Tournefier,[4] S. Tourneur,[40] K. Trabelsi,[40] M. Traill,[52] M. T. Tran,[40] M. Tresch,[41] A. Trisovic,[39] A. Tsaregorodtsev,[6] P. Tsopelas,[42] N. Tuning,[42,39] A. Ukleja,[29] A. Ustyuzhanin,[66,65] U. Uwer,[12] C. Vacca,[16,39,j] V. Vagnoni,[15] G. Valenti,[15] A. Vallier,[7] R. Vazquez Gomez,[19] P. Vazquez Regueiro,[38] C. Vázquez Sierra,[38] S. Vecchi,[17] M. van Veghel,[43] J. J. Velthuis,[47] M. Veltri,[18,t] G. Veneziano,[40] M. Vesterinen,[12] B. Viaud,[7] D. Vieira,[2] M. Vieites Diaz,[38] X. Vilasis-Cardona,[37,e] V. Volkov,[33] A. Vollhardt,[41] D. Voong,[47] A. Vorobyev,[31] V. Vorobyev,[35] C. Voß,[64] J. A. de Vries,[42] R. Waldi,[64] C. Wallace,[49] R. Wallace,[13] J. Walsh,[24] J. Wang,[60] D. R. Ward,[48] N. K. Watson,[46] D. Websdale,[54] A. Weiden,[41] M. Whitehead,[39] J. Wicht,[49] G. Wilkinson,[56,39] M. Wilkinson,[60] M. Williams,[39] M. P. Williams,[46] M. Williams,[57] T. Williams,[46] F. F. Wilson,[50] J. Wimberley,[59] J. Wishahi,[10] W. Wislicki,[29] M. Witek,[27] G. Wormser,[7] S. A. Wotton,[48] K. Wraight,[52] S. Wright,[48] K. Wyllie,[39] Y. Xie,[62] Z. Xu,[40] Z. Yang,[3] J. Yu,[62] X. Yuan,[35] O. Yushchenko,[36] M. Zangoli,[15] M. Zavertyaev,[11,u] L. Zhang,[3] Y. Zhang,[3] A. Zhelezov,[12] A. Zhokhov,[32] L. Zhong,[3] V. Zhukov,[9] and S. Zucchelli[15]

(LHCb Collaboration)

[1]*Centro Brasileiro de Pesquisas Físicas (CBPF), Rio de Janeiro, Brazil*
[2]*Universidade Federal do Rio de Janeiro (UFRJ), Rio de Janeiro, Brazil*

[3]*Center for High Energy Physics, Tsinghua University, Beijing, China*
[4]*LAPP, Université Savoie Mont-Blanc, CNRS/IN2P3, Annecy-Le-Vieux, France*
[5]*Clermont Université, Université Blaise Pascal, CNRS/IN2P3, LPC, Clermont-Ferrand, France*
[6]*CPPM, Aix-Marseille Université, CNRS/IN2P3, Marseille, France*
[7]*LAL, Université Paris-Sud, CNRS/IN2P3, Orsay, France*
[8]*LPNHE, Université Pierre et Marie Curie, Université Paris Diderot, CNRS/IN2P3, Paris, France*
[9]*I. Physikalisches Institut, RWTH Aachen University, Aachen, Germany*
[10]*Fakultät Physik, Technische Universität Dortmund, Dortmund, Germany*
[11]*Max-Planck-Institut für Kernphysik (MPIK), Heidelberg, Germany*
[12]*Physikalisches Institut, Ruprecht-Karls-Universität Heidelberg, Heidelberg, Germany*
[13]*School of Physics, University College Dublin, Dublin, Ireland*
[14]*Sezione INFN di Bari, Bari, Italy*
[15]*Sezione INFN di Bologna, Bologna, Italy*
[16]*Sezione INFN di Cagliari, Cagliari, Italy*
[17]*Sezione INFN di Ferrara, Ferrara, Italy*
[18]*Sezione INFN di Firenze, Firenze, Italy*
[19]*Laboratori Nazionali dell'INFN di Frascati, Frascati, Italy*
[20]*Sezione INFN di Genova, Genova, Italy*
[21]*Sezione INFN di Milano Bicocca, Milano, Italy*
[22]*Sezione INFN di Milano, Milano, Italy*
[23]*Sezione INFN di Padova, Padova, Italy*
[24]*Sezione INFN di Pisa, Pisa, Italy*
[25]*Sezione INFN di Roma Tor Vergata, Roma, Italy*
[26]*Sezione INFN di Roma La Sapienza, Roma, Italy*
[27]*Henryk Niewodniczanski Institute of Nuclear Physics Polish Academy of Sciences, Kraków, Poland*
[28]*AGH - University of Science and Technology, Faculty of Physics and Applied Computer Science, Kraków, Poland*
[29]*National Center for Nuclear Research (NCBJ), Warsaw, Poland*
[30]*Horia Hulubei National Institute of Physics and Nuclear Engineering, Bucharest-Magurele, Romania*
[31]*Petersburg Nuclear Physics Institute (PNPI), Gatchina, Russia*
[32]*Institute of Theoretical and Experimental Physics (ITEP), Moscow, Russia*
[33]*Institute of Nuclear Physics, Moscow State University (SINP MSU), Moscow, Russia*
[34]*Institute for Nuclear Research of the Russian Academy of Sciences (INR RAN), Moscow, Russia*
[35]*Budker Institute of Nuclear Physics (SB RAS) and Novosibirsk State University, Novosibirsk, Russia*
[36]*Institute for High Energy Physics (IHEP), Protvino, Russia*
[37]*Universitat de Barcelona, Barcelona, Spain*
[38]*Universidad de Santiago de Compostela, Santiago de Compostela, Spain*
[39]*European Organization for Nuclear Research (CERN), Geneva, Switzerland*
[40]*Ecole Polytechnique Fédérale de Lausanne (EPFL), Lausanne, Switzerland*
[41]*Physik-Institut, Universität Zürich, Zürich, Switzerland*
[42]*Nikhef National Institute for Subatomic Physics, Amsterdam, The Netherlands*
[43]*Nikhef National Institute for Subatomic Physics and VU University Amsterdam, Amsterdam, The Netherlands*
[44]*NSC Kharkiv Institute of Physics and Technology (NSC KIPT), Kharkiv, Ukraine*
[45]*Institute for Nuclear Research of the National Academy of Sciences (KINR), Kyiv, Ukraine*
[46]*University of Birmingham, Birmingham, United Kingdom*
[47]*H.H. Wills Physics Laboratory, University of Bristol, Bristol, United Kingdom*
[48]*Cavendish Laboratory, University of Cambridge, Cambridge, United Kingdom*
[49]*Department of Physics, University of Warwick, Coventry, United Kingdom*
[50]*STFC Rutherford Appleton Laboratory, Didcot, United Kingdom*
[51]*School of Physics and Astronomy, University of Edinburgh, Edinburgh, United Kingdom*
[52]*School of Physics and Astronomy, University of Glasgow, Glasgow, United Kingdom*
[53]*Oliver Lodge Laboratory, University of Liverpool, Liverpool, United Kingdom*
[54]*Imperial College London, London, United Kingdom*
[55]*School of Physics and Astronomy, University of Manchester, Manchester, United Kingdom*
[56]*Department of Physics, University of Oxford, Oxford, United Kingdom*
[57]*Massachusetts Institute of Technology, Cambridge, Massachusetts, USA*
[58]*University of Cincinnati, Cincinnati, Ohio, USA*
[59]*University of Maryland, College Park, Maryland, USA*
[60]*Syracuse University, Syracuse, New York, USA*

[61]*Pontifícia Universidade Católica do Rio de Janeiro (PUC-Rio), Rio de Janeiro, Brazil (associated with Universidade Federal do Rio de Janeiro (UFRJ), Rio de Janeiro, Brazil)*
[62]*Institute of Particle Physics, Central China Normal University, Wuhan, Hubei, China (associated with Center for High Energy Physics, Tsinghua University, Beijing, China)*
[63]*Departamento de Fisica, Universidad Nacional de Colombia, Bogota, Colombia (associated with LPNHE, Université Pierre et Marie Curie, Université Paris Diderot, CNRS/IN2P3, Paris, France)*
[64]*Institut für Physik, Universität Rostock, Rostock, Germany (associated with Physikalisches Institut, Ruprecht-Karls-Universität Heidelberg, Heidelberg, Germany)*
[65]*National Research Centre Kurchatov Institute, Moscow, Russia (associated with Institute of Theoretical and Experimental Physics (ITEP), Moscow, Russia)*
[66]*Yandex School of Data Analysis, Moscow, Russia (associated with Institute of Theoretical and Experimental Physics (ITEP), Moscow, Russia)*
[67]*Instituto de Fisica Corpuscular (IFIC), Universitat de Valencia-CSIC, Valencia, Spain (associated with Universitat de Barcelona, Barcelona, Spain)*
[68]*Van Swinderen Institute, University of Groningen, Groningen, The Netherlands (associated with Nikhef National Institute for Subatomic Physics, Amsterdam, The Netherlands)*

[†]Deceased.
[a]Also at Università di Ferrara, Ferrara, Italy.
[b]Also at Università della Basilicata, Potenza, Italy.
[c]Also at Università di Milano Bicocca, Milano, Italy.
[d]Also at Università di Modena e Reggio Emilia, Modena, Italy.
[e]Also at LIFAELS, La Salle, Universitat Ramon Llull, Barcelona, Spain.
[f]Also at Università di Bologna, Bologna, Italy.
[g]Also at Università di Roma Tor Vergata, Roma, Italy.
[h]Also at Università di Genova, Genova, Italy.
[I]Also at Scuola Normale Superiore, Pisa, Italy.
[j]Also at Università di Cagliari, Cagliari, Italy.
[k]Also at Università di Padova, Padova, Italy.
[l]Also at Laboratoire Leprince-Ringuet, Palaiseau, France.
[m]Also at Universidade Federal do Triângulo Mineiro (UFTM), Uberaba-MG, Brazil.
[n]Also at AGH - University of Science and Technology, Faculty of Computer Science, Electronics and Telecommunications, Kraków, Poland.
[o]Also at Hanoi University of Science, Hanoi, Viet Nam.
[p]Also at Università di Bari, Bari, Italy.
[q]Also at Università degli Studi di Milano, Milano, Italy.
[r]Also at Università di Roma La Sapienza, Roma, Italy.
[s]Also at Università di Pisa, Pisa, Italy.
[t]Also at Università di Urbino, Urbino, Italy.
[u]Also at P.N. Lebedev Physical Institute, Russian Academy of Science (LPI RAS), Moscow, Russia.